ACS Pharmacology & Translational Science

pubs.acs.org/ptsci Article

Mapping the Molecular Surface of the Analgesic $Na_V1.7$-Selective Peptide Pn3a Reveals Residues Essential for Membrane and Channel Interactions

Alexander Mueller, Zoltan Dekan, Quentin Kaas, Akello J. Agwa, Hana Starobova, Paul F. Alewood, Christina I. Schroeder, Mehdi Mobli, Jennifer R. Deuis,* and Irina Vetter*

Cite This: *ACS Pharmacol. Transl. Sci.* 2020, 3, 535−546 Read Online

ACCESS | Metrics & More | Article Recommendations | Supporting Information

ABSTRACT: Compelling human genetic studies have identified the voltage-gated sodium channel $Na_V1.7$ as a promising therapeutic target for the treatment of pain. The analgesic spider-venom-derived peptide μ-theraphotoxin-Pn3a is an exceptionally potent and selective inhibitor of $Na_V1.7$; however, little is known about the structure−activity relationships or channel interactions that define this activity. We rationally designed 17 Pn3a analogues and determined their activity at $hNa_V1.7$ using patch−clamp electrophysiology. The positively charged amino acids K22 and K24 were identified as crucial for Pn3a activity, with molecular modeling identifying interactions of these residues with the S3−S4 loop of domain II of $hNa_V1.7$. Removal of hydrophobic residues Y4, Y27, and W30 led to a loss of potency (>250-fold), while replacement of negatively charged D1 and D8 residues with a positively charged lysine led to increased potencies (>13-fold), likely through alterations in membrane lipid interactions. Mutating D8 to an asparagine led to the greatest improvement in Pn3a potency at $Na_V1.7$ (20-fold), while maintaining >100-fold selectivity over the major off-targets $Na_V1.4$, $Na_V1.5$, and $Na_V1.6$. The Pn3a[D8N] mutant retained analgesic activity *in vivo*, significantly attenuating mechanical allodynia in a clinically relevant mouse model of postsurgical pain at doses 3-fold lower than those with wild-type Pn3a, without causing motor-adverse effects. Results from this study will facilitate future rational design of potent and selective peptidic $Na_V1.7$ inhibitors for the development of more efficacious and safer analgesics as well as to further investigate the involvement of $Na_V1.7$ in pain.

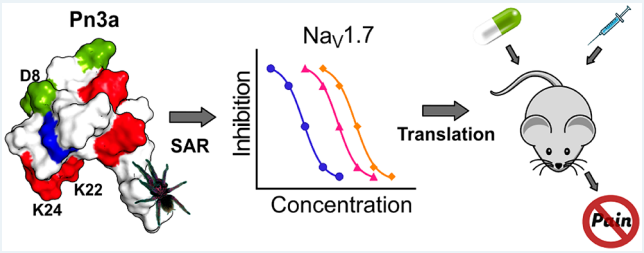

KEYWORDS: *structure−activity relationship, peptide synthesis, voltage-gated sodium channel 1.7, gating-modifier toxin, pharmacophore, pain*

1. INTRODUCTION

Pain remains a poorly treated condition with currently used analgesics often suffering from poor tolerability, abuse potential, or lack of broad efficacy.[1] The voltage-gated sodium channel isoform $Na_V1.7$ is considered one of the most promising validated pain targets, with loss-of-function mutations leading to Congenital Insensitivity to Pain (CIP),[2] while gain-of-function mutations are associated with a range of painful conditions.[3−5] As CIP is characterized by a lack of nociception, with no other significant autonomic or sensory impairments apart from anosmia,[6] targeting $Na_V1.7$ pharmacologically promises to deliver effective analgesia without substantial side effects. Accordingly, intense research efforts have been devoted to the identification of subtype-selective $Na_V1.7$ modulators.[7,8] Nevertheless, this endeavor has proven challenging, not the least owing to the high degree of similarity of the Na_V subtypes, especially in the pore domain where many clinically used Na_V modulators bind.[6]

One particularly promising source of selective Na_V modulators are animal venoms, which are typically dominated by small (~20−40 amino acids) peptides that target the voltage-sensing domains (VSDs) of Na_V channels.[9−11] Specifically, several spider-venom-derived peptides target the VSDII to stabilize the "down" or resting/closed state of the channel, leading to a depolarizing shift in the voltage-dependence of channel activation.[12,13] Analogous to small molecules binding to VSDIV of $Na_V1.7$,[14] targeting the voltage sensors of domain II imparts a typically greater degree of selectivity compared to targeting the pore domain, with many spider-venom-derived peptides displaying excellent selectivity

Received: January 7, 2020
Published: February 19, 2020

https://dx.doi.org/10.1021/acsptsci.0c00002
ACS Pharmacol. Transl. Sci. 2020, 3, 535−546

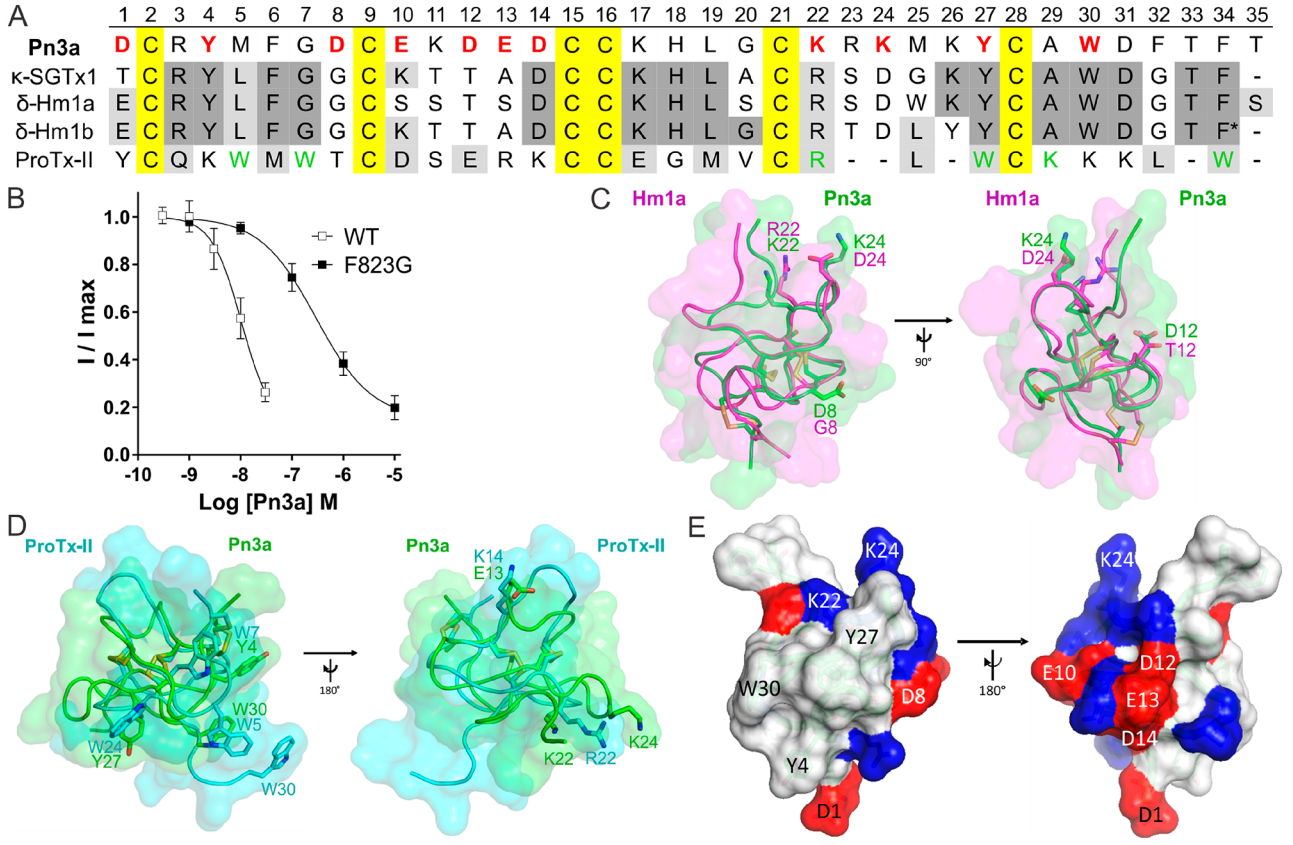

Figure 1. Sequence and structural features of Pn3a (A) Amino acid sequence alignment of Pn3a with closely related venom peptides κ-SGTx1, δ-Hm1a, δ-Hm1b, and ProTx-II. Yellow shading indicates cysteines; dark gray and light gray shading represent identical and similar amino acids, respectively, compared to Pn3a. Red bold letters indicate residues included in SAR study; green letters indicate pharmacophore residues in ProTx-II for $Na_V1.7$ activity.[12,30,31] * indicates amidated C-terminus of Hm1b. (B) Pn3a is 28-fold more potent at wild-type $mNa_V1.7$ (IC_{50} 10.4 nM) compared to $mNa_V1.7$[F823G] (IC_{50} 293.4 nM) mutant channels assessed by whole-cell patch−clamp experiments. Data are presented as mean ± SEM, with n = 5−9 cells per data point. (C) Comparison of NMR structures of Pn3a (Protein Databank (PDB) 5T4R; green) with Hm1a (PDB 2N6O; pink) superimposed over the disulfide bonds (yellow), generated with PyMol. Residues of interest are labeled and shown in stick representation. (D) Comparison of NMR structures of Pn3a (PDB 5T4R; green) with ProTx-II (PDB 2N9T; cyan) superimposed over the disulfide bonds (yellow). Overlapping residues with similar chemical properties are labeled and shown as sticks. (E) Surface structure of Pn3a with acidic and basic residues highlighted in red and blue, respectively. The hydrophobic patch (including W30, Y4, and Y27) is surrounded by a charged ring (including D1, D8, K22, and K24; left), while the reverse side is hydrophilic with mainly charged side chains (right). Only residues included in this SAR study are labeled.

over tetrodotoxin (TTX)-resistant isoforms including the cardiac isoform $Na_V1.5$, a major pharmacological off-target.[6] However, selectivity for $Na_V1.7$ over the TTX-sensitive isoforms is often more limited, with few potent and truly selective molecules reported.[15−17] These include the prototypical $Na_V1.7$-targeting peptide toxin Protoxin-II (ProTx-II or β/ω-theraphotoxin-Tp2a) from the venom of the tarantula *Thrixopelma pruriens*[18] and rationally engineered analogues of Jingzhaotoxin-V (JzTx-V, β/κ-theraphotoxin-Cg2a)[19] and GpTx-1 (ω-theraphotoxin-Gr2a),[20] as well as the recently described analgesic peptide Pn3a (μ-theraphotoxin-Pn3a) from the venom of the tarantula *Pamphobeteus nigricolor*.[21,22] Notably, these $Na_V1.7$ inhibitors belong to diverse peptide families of Na_V channel targeting spider venom toxins (NaSpTx families 1−3), based on sequence similarities.[17,23] Extensive structure−activity studies have been described for NaSpTx family 3 peptides, which include JzTx-V and ProTx-II,[17,19,24,25] as well as for NaSpTx family 1 peptides, which include GpTx-1.[17,20,26] However, so far nothing is known about the structural features that confer activity at $Na_V1.7$ for the NaSpTx family 2 peptides, to which Pn3a belongs. Pn3a is one of the most potent and selective reported $Na_V1.7$ blockers and inhibits $Na_V1.7$ with several hundred fold selectivity over the key TTX-sensitive off-targets $Na_V1.4$ and $Na_V1.6$ and it is analgesic either alone or in combination with oxycodone or baclofen in multiple animal models of pain.[21,22]

Thus, the goal of this study was to investigate the structure−activity relationships of Pn3a using rational analogue design to better understand the features necessary for potent inhibition of $Na_V1.7$. We confirmed the importance of a key phenylalanine residue near the S3−S4 loop of $Na_V1.7$ VSDII (F823) for peptide activity and identified several Pn3a amino acid residues crucial for potency, selectivity and membrane binding. Improved *in vivo* antinociceptive efficacy of Pn3a[D8N] was confirmed in a $Na_V1.7$ target engagement assay as well as a mouse model of postsurgical pain. These results will guide future rational design of potent and selective $Na_V1.7$ inhibitors as more efficacious and safer analgesics.

2. RESULTS AND DISCUSSION

2.1. F823 in VSDII of $Na_V1.7$ Is a Key Residue for Interaction with Pn3a. To date, Pn3a is the only reported $Na_V1.7$-selective inhibitor belonging to NaSpTx family 2, with

https://dx.doi.org/10.1021/acsptsci.0c00002
ACS Pharmacol. Transl. Sci. 2020, 3, 535−546

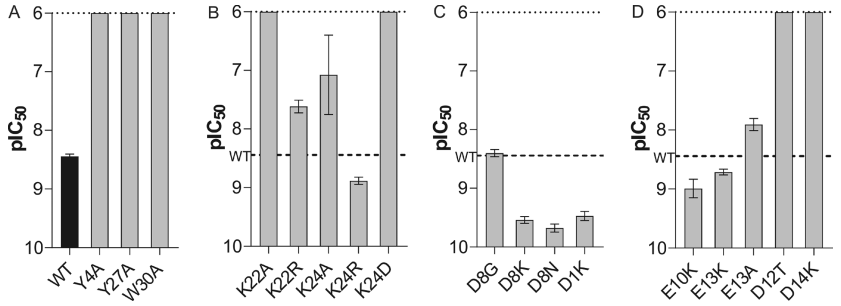

Figure 2. Activity of Pn3a mutants at hNa$_V$1.7 assessed by whole-cell patch−clamp experiments. (A) Potency of Pn3a (WT) and the surface hydrophobic patch analogues Y4A, Y27A, and W30A. Y27A is in a non-native fold. (B) Potency of analogues with mutations at position 22 and 24. (C) Potency of charged ring analogues D8G, D8K, D8N, and D1K. (D) Potency of Pn3a analogues E10K, E13K, E13A, D12T, and D14K. D12T and D14K are in a non-native fold. The dotted line indicates the maximal tested concentration of 1 μM. The dashed line indicates the potency of wild-type Pn3a. Data are presented as mean ± SEM, with n = 3−9 cells per data point.

most other members of this family inhibiting voltage-gated potassium (K$_V$) channels, or acting as functional Na$_V$ activators. Specifically, the NaSpTx family 2 Na$_V$ modulator most closely related to Pn3a is SGTx1 (κ-theraphotoxin-Scg1a), sharing 22 identical residues and a very similar 3D backbone structure, which is a nonselective Na$_V$ activator and K$_V$2.1 inhibitor[27,28] (Figure 1A). Similarly, the closely related family 2 peptides Hm1a and Hm1b (δ-theraphotoxin-Hm1a and δ-theraphotoxin-Hm1b) selectively inhibit inactivation of Na$_V$1.1 but have no effect on Na$_V$1.7[29] (Figure 1A). In contrast, the spider-venom-derived peptide most pharmacologically similar to Pn3a is ProTx-II, a selective NaSpTx family 3 Na$_V$1.7 blocker with a well-described pharmacophore.[12,30,31] However, ProTx-II has little sequence similarity to Pn3a (Figure 1A), and although we have previously demonstrated that Na$_V$1.7 inhibition by Pn3a involves binding to the S3−S4 loop of VSDII, we first sought to verify that Pn3a and ProTx-II share an overlapping binding site. ProTx-II has previously been shown to bind to F823 (mNa$_V$1.7; F813 hNa$_V$1.7) in the S3−S4 loop of VSDII (ELFLADVEG), with a F823→G mutation reducing ProTx-II inhibitory activity by between 9- and 100-fold.[18,32] This interaction was also confirmed by recent structural studies[12] which additionally suggest that besides van der Waals interactions of F823 with hydrophobic ProTx-II residues this Na$_V$1.7-specific residue may be important for S3 helix stabilization as well as for S3−S4 loop orientation in VSDII to provide a Na$_V$1.7-specific receptor site.

We therefore assessed the potency of Pn3a at a F823G mutant of Na$_V$1.7 and found that as expected Pn3a was 28-fold less active at mutant (IC$_{50}$ 293.4 nM) channels compared to wild-type channels (IC$_{50}$ 10.4 nM) (Figure 1B), suggesting an overlapping binding site of Pn3a and ProTx-II at VSDII.

2.2. Comparison of the Primary and Tertiary Structure of Pn3a to Spider Venom-Derived Na$_V$ Modulators. To identify amino acids that might confer Na$_V$1.7-selective inhibition, we used a systematic approach based on aligning and comparing the primary (Figure 1A) and tertiary structures of Pn3a with structurally closely related spider venom peptides (SGTx1, Hm1a, and Hm1b) (Figure 1C) as well as the pharmacologically similar ProTx-II (Figure 1D), despite obvious differences in the sequences. Our sequence and structural alignments revealed several interesting commonalities and differences, including several charge substitutions in Pn3a compared to Hm1b and ProTx-II (D8, D12, E10, E13, and K24), as well as a structurally conserved arrangement of key aromatic residues (Y4, Y27, and W30) (Figure 1A,D). Thus, overall, Pn3a has a conserved amphipathic surface structure with a hydrophobic patch surrounded by charged residues (Figure 1E), which is thought to permit membrane partitioning as well as interaction with parts of the VSDs located close to the extracellular surface.[12,33,34] Therefore, to delineate the contributions of these residues to Pn3a activity, we next pharmacologically characterized select peptide analogues.

2.3. Conserved Hydrophobic Patch of Pn3a Contributes to Activity and Peptide Folding. On the basis of the observed overlap of Y4, Y27, and W30 in Pn3a with W7, W24, and W5, respectively, in ProTx-II (Figure 1D), we first characterized the contribution of these hydrophobic patch residues to Pn3a activity. Mutations of all three residues to alanine resulted in at least 250-fold reduced potency against Na$_V$1.7 (IC$_{50}$ values >1 μM) compared to Pn3a (IC$_{50}$ 4 nM) (Figure 2A, Table 1), although the isolated predominant isomer obtained for Pn3a[Y27A] was in a non-native fold as determined by 1D NMR (Figure S1). A similar contribution of

Table 1. Potency of Pn3a Analogues at hNa$_V$1.7[a]

Pn3a analogue	pIC$_{50}$ [M]	IC$_{50}$ [nM]
WT	8.45 ± 0.04	4
D1K	9.47 ± 0.08	0.3
Y4A	<6	>1000
D8K	9.54 ± 0.06	0.3
D8N	9.68 ± 0.07	0.2
D8G	8.40 ± 0.06	4
E10K	8.99 ± 0.16	1
D12T[b]	<6	>1000
E13K	8.71 ± 0.05	2
E13A	7.91 ± 0.10	12
D14K[b]	<6	>1000
K22A	<6	>1000
K22R	7.62 ± 0.11	24
K24A	7.08 ± 0.68	84
K24D	<6	>1000
K24R	8.88 ± 0.06	1
Y27A[b]	<6	>1000
W30A	<6	>1000

[a]pIC$_{50}$ (expressed as mean ± SEM) and IC$_{50}$ values of Pn3a (WT) and Pn3a-analogues derived from concentration-response relationships assessed by whole-cell patch−clamp experiments [b]Non-native fold assessed by 1D NMR; all other analogues showed the same fold as WT peptide

https://dx.doi.org/10.1021/acsptsci.0c00002
ACS Pharmacol. Transl. Sci. 2020, 3, 535−546

this residue to folding of SGTx1 has previously been reported, with the SGTx1[Y27A] mutant lowering folding efficiency and preventing identification of a correctly folded peptide.[35] Interestingly, hydrophobic patch residues are also critical for the potency of ProTx-II and appear to anchor the peptide in the membrane-embedded lipophilic cleft at the S2 and S3 interface just above F813 of VSDII in hNa$_V$1.7.[12,31] These results suggest that Pn3a may employ a binding mode similar to that of ProTx-II with hydrophobic patch residues directly interacting with Na$_V$1.7 and confirms Y4 and W30 as part of the pharmacophore and Y27 as important structural feature for native folding of Pn3a.

2.4. K22 and a Basic Residue at Position 24 Are Essential for Inhibition of Na$_V$1.7. R22 in ProTx-II is critical for its potency and has been shown to directly interact with acidic residues in the extracellular S3−S4 loop of Na$_V$1.7 VSDII, antagonizing S4 gating-charge movement to prevent channel opening.[12] Interestingly, K22 and K24 in Pn3a flank the corresponding position of R22 in ProTx-II and are located in close proximity, although neither directly overlap with this crucial pharmacophore residue (Figure 1D). We therefore assessed activity of charge-neutral K22 and K24 analogues (K22A and K24A) as well as the corresponding arginine mutants (K22R and K24R) and the negatively charged analogue (K24D) which additionally mirrors the sequence of the family 2 Na$_V$ activators SGTx1, Hm1a and Hm1b in this position (Figure 1A,C).

As expected, both K24A (IC$_{50}$ 84 nM) and K22A (IC$_{50}$ > 1 μM) lost activity against Na$_V$1.7, although substitution of K24 appears better tolerated than replacement of K22, with 21- and >250-fold loss of potency, respectively (Figure 2B, Table 1). Similarly, substitution of K22 with arginine led to a 6-fold decrease in potency (IC$_{50}$ 24 nM), while K24R (IC$_{50}$ 1 nM) gained 4-fold potency compared to that of Pn3a, suggesting that the lysine at position 22 and a basic residue at position 24 in Pn3a are important for potent Na$_V$1.7 channel inhibition (Figure 2B, Table 1). The bulkier arginine at position 22 in Pn3a may be sterically unfavorable for channel engagement, while position 24 seems more tolerant to modifications. Na$_V$1.7 may better accommodate an arginine at position 24 for more potent channel inhibition.

Interestingly, the Na$_V$ activators SGTx1, Hm1a, and Hm1b all contain an aspartic acid at position 24 (Figure 1A), suggesting this residue may be an important feature for the different pharmacological profiles. Indeed, consistent with a voltage-sensor trapping model involving electrostatic interactions between charged residues of toxins and the VSD, we hypothesized that the K24D substitution might impart Na$_V$ activator properties on Pn3a. However, while the Pn3a[K24D] analogue lost >250-fold potency at Na$_V$1.7 (IC$_{50}$ > 1 μM) (Figure 2B, Table 1), we neither observed increases in peak currents, hyperpolarizing shifts in the voltage-dependence of activation, or delayed inactivation at either Na$_V$1.1 and Na$_V$1.7 channels (Figure S2). Given that effects on inactivation are typically mediated via interaction with the VSD of domain IV, while effects on activation are commonly mediated via VSDII interactions, it is perhaps not surprising that this single-residue substitution did not convert Pn3a into a Na$_V$ activator but only prevented potent inhibition of channel activation. Further VSDIV interactions that would interfere with channel inactivation (similar to SGTx1, Hm1a, and Hm1b effects) may require additional mutations to Pn3a. Nevertheless, our findings indicate that the presence of D24 in Hm1a/b and SGTx1 may prevent these peptides from being Na$_V$ channel blockers by preventing close interaction with acidic VSDII S3−S4 loop residues. Indeed, the D24A mutation in SGTx1 has been shown to result in a ∼20-fold reduction of the K_d value compared to that of wild-type peptide.[35] Future studies are needed to investigate if a single amino acid exchange to a basic residue at position 24 can turn these Na$_V$ activators into blockers.

2.5. Removal of Negative Charges Improves Pn3a Potency. Pn3a contains a number of negatively charged residues differentiating it from both the NaSpTx family 2 Na$_V$ activators as well as ProTx-II, including D1, D8, E10, D12, E13, and D14 (Figure 1A). To explore the contributions of these residues to Pn3a activity, we generated a range of analogues based on charge neutralizing or charge reversing substitutions. Pn3a[D8G], analogous to the corresponding residue in SGTx1, Hm1a, and Hm1b, remained equipotent (IC$_{50}$ 4 nM) in patch−clamp experiments. Surprisingly, D8N (IC$_{50}$ 0.2 nM) and D8K (IC$_{50}$ 0.3 nM) displayed a 20- and 13-fold improved potency at Na$_V$1.7 compared to wild-type Pn3a, respectively (Figure 2C, Table 1). This suggests that a positive or polar-neutral residue at position 8 in Pn3a allows for better inhibition of the channel, possibly due to facilitation of direct Na$_V$ channel interactions or through advantageous membrane binding properties. Similarly, the potency of Pn3a[D1K] (IC$_{50}$ 0.3 nM) was improved 13-fold (Figure 2C, Table 1).

The position corresponding to Pn3a E10 is occupied by a lysine residue in Hm1b, while E13 in Pn3a overlays well with the oppositely charged K14 in ProTx-II and an alanine residue in Hm1b (Figure 1A,D). We therefore also generated E10K, E13K, and E13A Pn3a analogues. The nature of the residues at position 10 and 13 did not have a large impact on activity, as E10K (IC$_{50}$ 1 nM), E13K (IC$_{50}$ 2 nM), and E13A (IC$_{50}$ 12 nM) had only 4- and 2-fold improvement and 3-fold decrease in potency at Na$_V$1.7, respectively (Figure 2D, Table 1).

We also generated D12T and D14K analogues based on similarity to Hm1a and ProTx-II, respectively, but we found that these analogues did not adopt the native fold (Figure S1) and were inactive at Na$_V$1.7 up to 1 μM (Figure 2D, Table 1). The NMR solution structure of Pn3a (PDB 5T4R) suggests a possible salt bridge between D12 and R23 as well as hydrogen bonds of D14 with the K11 side chain and the backbone amide hydrogens of E10 and K11 (Figure S3), suggesting that the side chains of D12 and D14 are important for the stability of the correct fold. This might explain the low synthetic folding yields of Hm1a and Hm1b, which required regioselective disulfide bond formation to produce useful quantities.[29] In contrast, Pn3a can be synthesized using a nonselective approach with reasonable yield.

In summary, six mutations (D1K, D8N, D8K, E10K, E13K, and K24R) were identified that resulted in improved potency at hNav1.7. Furthermore, four amino acids (Y4, K22, K24, and W30) were shown to be an important part of the pharmacophore of Pn3a for potent Na$_V$1.7 inhibition and three residues (D12, D14, and Y27) were identified as important for folding of Pn3a into its native and active inhibitor cysteine knot (ICK) structure.

2.6. Selectivity of Pn3a Analogues with Improved Potency at Na$_V$1.7. We next estimated the Na$_V$1.1−1.8 selectivity of the Pn3a analogues with improved potency at Na$_V$1.7 using a high-throughput fluorescence-based assay, to assess the impact of these mutations on the potency at other Na$_V$ channel isoforms. The rank order of selectivity for Na$_V$1.7

https://dx.doi.org/10.1021/acsptsci.0c00002
ACS Pharmacol. Transl. Sci. 2020, 3, 535−546

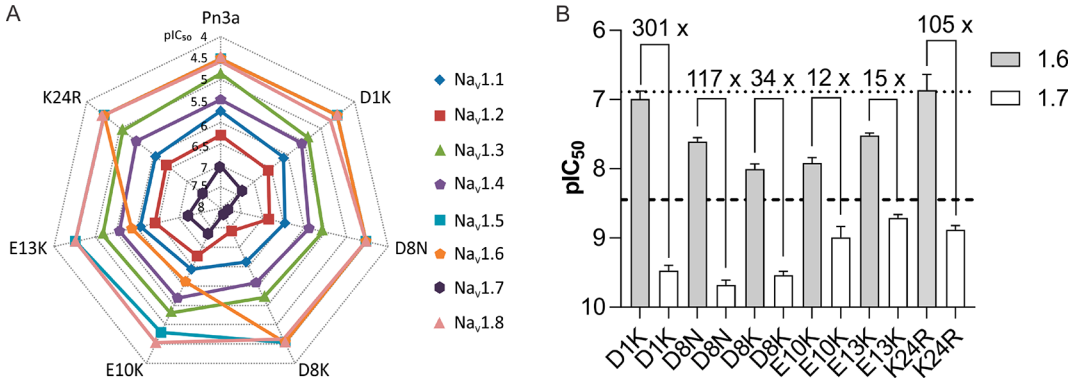

Figure 3. $Na_V1.1-1.8$ selectivity of Pn3a analogues with improved potency at $Na_V1.7$. (A) Potency at $hNa_V1.1-1.8$ represented on a radar plot assessed using fluorescence-based assays with membrane potential dye. Data is presented as the pIC_{50} averaged from 3 independent replicates (each with 3 identical wells per treatment). (B) Comparative potency of select Pn3a analogues at $hNa_V1.6$ and $hNa_V1.7$ assessed by whole-cell patch−clamp experiments. Numbers above bars indicate fold selectivity for $Na_V1.7$ over $Na_V1.6$. Dashed and dotted lines indicate potencies of wild-type Pn3a at $Na_V1.7$ and $Na_V1.6$, respectively (values for $Na_V1.6$ are those previously reported).[21] Data are presented as mean ± SEM; n = 4−7 cells.

($Na_V1.7$ > $Na_V1.2$ > $Na_V1.1$ > $Na_V1.4$ > $Na_V1.3$ > $Na_V1.8$ ≥ $Na_V1.5$ = $Na_V1.6$) (see Table S1 for full selectivity values) was maintained for all analogues except E10K and E13K, which gained potency at $Na_V1.6$ (Figure 3A, Table S1).

In the peripheral nervous system, $Na_V1.6$ expression is highly localized to the nodes of Ranvier, where it contributes to the saltatory conduction of action potentials on both myelinated sensory and motor neurons.[36] This makes $Na_V1.6$ a major off-target for peripherally restricted Na_V channel blockers, as pharmacological inhibition of $Na_V1.6$ will likely cause intolerable motor-adverse effects.[37,38] We therefore assessed the potency of Pn3a analogues with improved potency at $Na_V1.7$ at $Na_V1.6$ using patch−clamp electrophysiology. Wild-type Pn3a inhibits $Na_V1.6$ with an IC_{50} of 129 nM, making it at least 100-fold selective for $Na_V1.7$ over $Na_V1.6$.[21] This selectivity window was maintained for D1K, D8N, and K24R, which had $Na_V1.6$ IC_{50} values of 102, 25, and 137 nM, respectively (Figure 3B). D8K displayed an intermediate selectivity (34-fold) over $Na_V1.6$ with an IC_{50} of 10 nM. Relative to $Na_V1.7$, E10K and E13K gained the most potency at $Na_V1.6$, with IC_{50} values of 12 and 30 nM, respectively, indicating that E10 and E13 residues are important in Pn3a for imparting selectivity over $Na_V1.6$ (Figure 3B). This suggests that residues on the hydrophilic face, opposite to the hydrophobic "active" surface, can change peptide pharmacodynamics and should not be disregarded when attempting to engineer potent and selective ICK peptides. The changes in selectivity for $Na_V1.6$ determined using electrophysiology matched those estimated from the fluorescence-based assays, validating this high-throughput approach as a method for estimating Na_V selectivity.

2.7. Pn3a Analogues Effectively Engage $Na_V1.7$ *In Vivo*. We next assessed $Na_V1.7$ target engagement of Pn3a analogues following local and systemic administration using a previously validated mouse model of $Na_V1.7$-mediated pain induced by intraplantar (i.pl.) injection of the scorpion toxin OD1.[39] E10K and E13K were not tested *in vivo* due to their small selectivity window over $Na_V1.6$ (12- to 15-fold). The i.pl. injection of wild-type Pn3a (1 μM) partially reduced OD1-induced spontaneous pain behaviors (control: 89 ± 6 flinches; Pn3a: 42 ± 3 flinches; Figure 4A), confirming $Na_V1.7$ target engagement and inhibition at peripheral nerve terminals *in vivo*. At the same concentration, D1K, D8N, D8K, and K24R almost completely abolished OD1-induced pain behaviors,

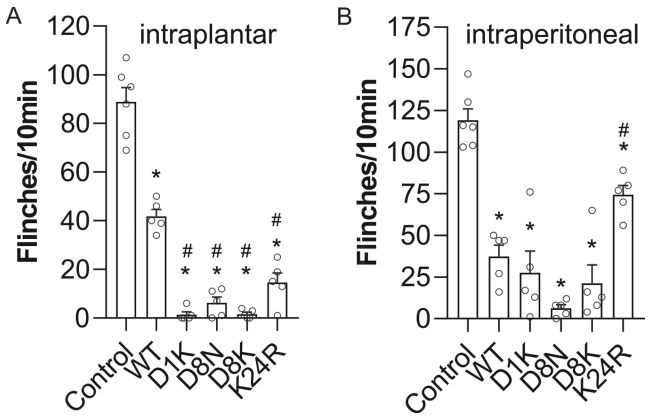

Figure 4. Comparative efficacy of Pn3a and analogues in a mouse model of $Na_V1.7$ mediated pain. (A) Local injection of Pn3a (WT) and analogues (i.pl., 1 μM) reverses spontaneous pain behaviors induced by i.pl. injection of the $Na_V1.7$ activator OD1 in mice; n = 5−6 per group. (B) Systemic administration of Pn3a (WT) and analogues (i.p., 1 mg/kg) reverses spontaneous pain behaviors induced by i.pl. injection of the $Na_V1.7$ activator OD1 in mice; n = 5−6 per group. Data are presented as mean ± SEM. Statistical significance was determined using one-way ANOVA with Dunnett's post-test; *, $p < 0.05$ compared to control, #, $p < 0.05$ compared to native Pn3a (WT).

consistent with their increased potency at $Na_V1.7$ *in vitro* (D1K: 2 ± 1 flinches; D8N: 6 ± 2 flinches; D8K: 2 ± 1 flinches; K24R: 15 ± 4 flinches; Figure 4A). We therefore next assessed systemic antinociceptive activity of the active Pn3a analogues. Following intraperitoneal (i.p.) injection, Pn3a D1K, D8N, D8K, and K24 (1 mg/kg) all significantly attenuated OD1-induced pain behaviors (control: 119 ± 7 flinches, Pn3a: 37 ± 7 flinches; D1K: 28 ± 13 flinches; D8N: 6 ± 2 flinches; D8K: 21 ± 11 flinches; K24R: 74 ± 6 flinches; Figure 4B), and D8N stood out as significantly more effective compared to Pn3a ($P < 0.05$, unpaired t test).

Despite being more potent than native Pn3a *in vitro*, K24R performed more poorly following systemic administration. A disconnection between *in vitro* potency and systemic *in vivo* efficacy is a common problem in the development of analgesic $Na_V1.7$ blockers (including small molecules and peptides), suggesting insufficient free plasma concentration or inaccessibility of relevant receptor sites.[6] Another possible explanation

https://dx.doi.org/10.1021/acsptsci.0c00002
ACS Pharmacol. Transl. Sci. 2020, 3, 535−546

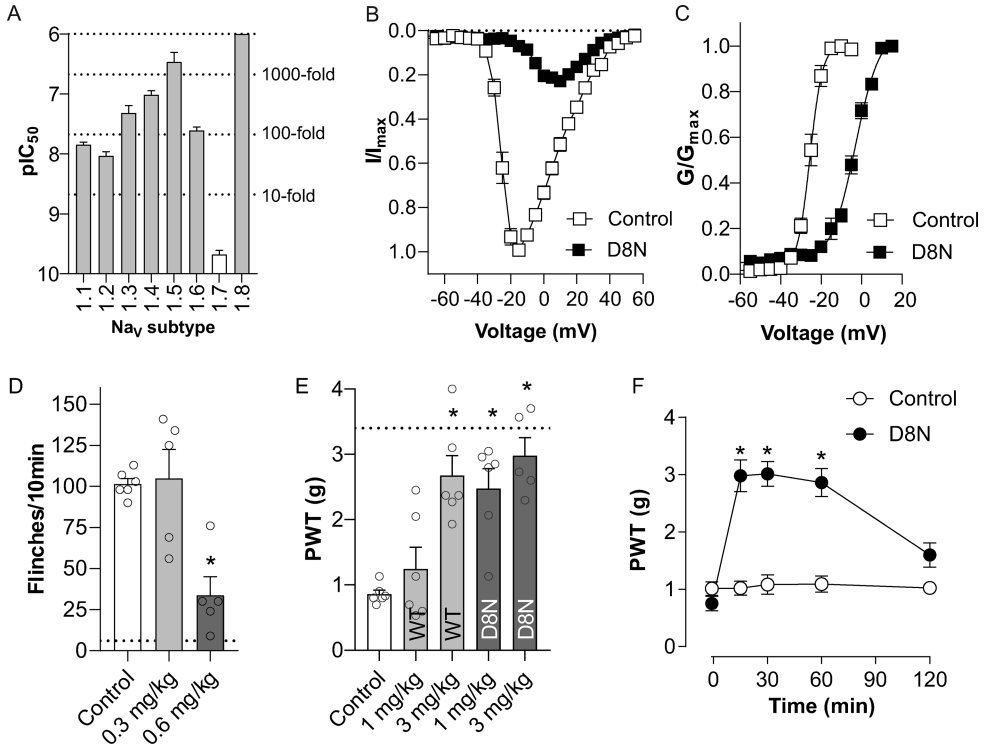

Figure 5. Pharmacological characterization of Pn3a[D8N] with improved potency at $Na_V1.7$. (A) Comparative potency of [D8N]Pn3a at $hNa_V1.1-1.8$ assessed by whole-cell patch−clamp experiments. [D8N]Pn3a most potently inhibited $Na_V1.7$ (IC_{50} 0.21 nM), with >40-fold selectivity over $Na_V1.1$ and $Na_V1.2$, >100-fold selectivity over $Na_V1.3$, $Na_V1.4$ and $Na_V1.6$, and >1000-fold selectivity over $Na_V1.5$ and $Na_V1.8$. (B) Current−voltage ($I-V$) relationship before and after addition of Pn3a[D8N] (100 nM) at $Na_V1.7$. (C) Conductance−voltage ($G-V$) relationship before and after addition of Pn3a[D8N] (100 nM) at $Na_V1.7$. Pn3a[D8N] shifted the voltage-dependence of activation by +22.4 mV. Data are presented as mean ± SEM, with n = 3−7 cells per data point. (D) Pn3a[D8N] (i.p.) dose-dependently reversed spontaneous pain behaviors induced by i.pl. injection of the $Na_V1.7$ activator OD1 in mice; n = 5−6 per group. The dotted line represents pain behaviors after i.p. injection of 1 mg/kg D8N. (E) Comparative efficacy of Pn3a (1 and 3 mg/kg i.p.) and Pn3a[D8N] (1 and 3 mg/kg i.p.) on postsurgical-pain-induced mechanical allodynia in mice; n = 5−6 per group. The dotted line represents mechanical thresholds of naïve mice. (F) Time course of reversal of postsurgical-pain-induced mechanical allodynia by Pn3a[D8N] (3 mg/kg i.p.); n = 5 per group. Data are presented as mean ± SEM. Statistical significance was determined using one-way or two-way ANOVA with Dunnett's post-test as appropriate; *, $p < 0.05$ compared to control.

may be the modest shift of the voltage-dependence of activation by K24R, which only caused a Δ +11.0 mV (from −22.62 to −11.67 mV) shift compared with a 21.3 mV shift for Pn3a (Figure S4). In summary, these results highlight D8N as the most potent Pn3a analogue *in vivo* after systemic administration and therefore as a promising analgesic lead compound for further assessment.

2.8. Pn3a[D8N] Maintains Selectivity for $Na_V1.7$ and Is a Potent Analgesic. Since Pn3a[D8N] showed improved potency at $Na_V1.7$ and was significantly more analgesic *in vivo* than wild-type Pn3a after systemic administration, we next sought to confirm selectivity over other Na_V subtypes using patch−clamp electrophysiology. Pn3a[D8N] exhibited similarly increased potencies across all of the Na_V subtypes when compared to native Pn3a, maintaining at least 100-fold selectivity over the major off-targets $Na_V1.4$, $Na_V1.5$, and $Na_V1.6$ (Figure 5A, Table 2). This increase in potency correlates with an increase in lipid membrane interactions (see Figure S5 and Table S2) suggesting that the removal of the negatively charged D8 residue drives overall potency via improved membrane affinity rather than by direct channel interactions. Indeed, membrane affinity seems to play an important role in the activity of Na_V blockers[40] and has been well-studied for ProTx-II and HwTx-IV.[31,33] The mechanism of $Na_V1.7$ channel block by Pn3a[D8N] remained the same as that for native Pn3a, with Pn3a[D8N] causing a large depolarizing shift in the voltage-dependence of activation (Δ +22.4 mV; from −25.51 mV to −3.09 mV), consistent with overlapping VSDII interactions (Figures 5B,C and S4). This closely matches the previously reported shift of Δ +21.3 mV of wild-type Pn3a[21] and further suggests that the D8N mutation does not change direct interactions of Pn3a with $Na_V1.7$ channels.

Table 2. Pn3a[D8N] and Pn3a Potency at $Na_V1.1$-1.8 and Selectivity for $Na_V1.7$[a]

	Pn3a[D8N]		Pn3a	
Na_V subtype	IC_{50} [nM]	$Na_V1.7$ selectivity	IC_{50} [nM]	$Na_V1.7$ selectivity
1.1	14	67	37	41
1.2	9	43	124	138
1.3	48	229	210	233
1.4	97	462	144	160
1.5	343	1633	800	889
1.6	25	119	129	143
1.7	0.21	1	0.9	1
1.8	>1000	>4762	>1000	>1111

[a]Data is presented as mean IC_{50} assessed by whole-cell patch−clamp experiments. Values for wild-type Pn3a are those previously reported.[21] The fold selectivity for $Na_V1.7$ over each other isoform was calculated as $IC_{50}(Na_V1.X)/IC_{50}(Na_V1.7)$.

https://dx.doi.org/10.1021/acsptsci.0c00002
ACS Pharmacol. Transl. Sci. 2020, 3, 535−546

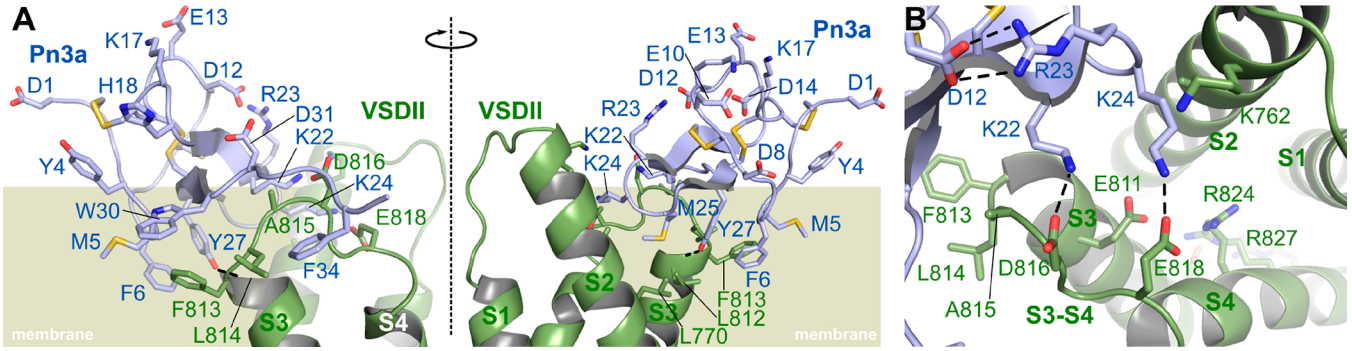

Figure 6. Molecular model of the interaction between Pn3a and $Na_V1.7$ VSDII down state. (A) Two cross-membrane views (180° rotated) of the interaction between the VSDII of Nav1.7 (green) and Pn3a (blue). The position of the lipid bilayer is indicated in olive green. (B) View parallel to the membrane showing the interaction of K22 and K24 with counter charges D816 and E818 in the S3−S4 segment. Only the side chains of selected residues are represented as sticks to increase readability. Hydrogen bonds that are discussed in the text are indicated by dashed lines. The VSDII is made of four α-helices noted as S1−S4. The molecular models were generated by homology using three templates: the cryo-EM structure of hNav1.7 VSDII-Na_VAb chimera in complex with ProTx-II (PDB 6N4R), the cryo-EM structure of hNav1.7 (PDB 6J8H), and the NMR solution structure of Pn3a (PDB 5T4R).

We next determined analgesic efficacy of systemic Pn3a-[D8N] doses using the OD1 model. Intraperitoneal administration of Pn3a[D8N] dose-dependently reduced OD1-induced flinching, with 1 mg/kg almost completely abolishing all spontaneous pain behaviors (Control: 102 ± 3; D8N 0.3 mg/kg: 105 ± 18; D8N 0.6 mg/kg: 34 ± 11; D8N 1 mg/kg: 6 ± 2; Figure 4B and 5**D**). We therefore took this dose forward into a clinically relevant model of postsurgical pain, in which $Na_V1.7$ inhibition was previously shown to be analgesic.[22] Pn3a[D8N] (1 mg/kg) significantly attenuated surgically induced mechanical allodynia (Control: 0.9 ± 0.1 g; Pn3a[D8N] 1 mg/kg: 2.5 ± 0.3 g), while native Pn3a at the same dose had no significant effect (Control: 0.9 ± 0.1 g; Pn3a 1 mg/kg: 1.2 ± 0.3 g), consistent with Pn3a[D8N] being more potent than native Pn3a at $Na_V1.7$ (Figure 5E). Analgesic doses of Pn3a (3 mg/kg) and Pn3a[D8N] (1 mg/kg) had no significant motor adverse effect as measured with the parallel rod floor test (ataxia index; control: 4.6 ± 0.8; Pn3a, 7.0 ± 1.5; Pn3a[D8N]: 6.9 ± 1.3; $P > 0.05$, one-way ANOVA), confirming the analgesic effects were not due to motor impairment. Increasing the dose of Pn3a[D8N] to 3 mg/kg resulted in full reversal of mechanical allodynia with withdrawal thresholds indifferent from those in healthy mice ($P > 0.05$, one-way ANOVA; Figure 5E) while still not causing motor impairments (ataxia index: 4.9 ± 1.5; $P > 0.05$ vs control, one-way ANOVA). The antinociceptive activity of systemically administered Pn3a[D8N] (3 mg/kg, i.p.) persisted for at least 1 h (Figure 5F), consistent with the expected short half-life due to rapid renal clearance that is typical for small globular peptides.[41,42]

2.9. Molecular Model of the Interaction between Pn3a and $Na_V1.7$ VSDII in the "Down" State. Recent advances in cryo-EM technology have made it possible to obtain high-resolution structures of human $Na_V1.7$ channels or chimeric $hNa_V1.7$(VSDII)-Na_VAb channels in complex with gating-modifier toxins bound to the voltage-sensing domains of the channel.[12,43] Particularly interesting was the high-resolution visualization of ProTx-II bound to VSDII in the putative "down"/closed state, the state that is preferentially bound and blocked by gating modifying channel inhibitors like Pn3a.[12] Since the binding site of Pn3a overlaps with that of ProTx-II (Figure 1B) and Pn3a shows several similarities in its pharmacophore compared to ProTx-II (Figure 1D), we used this cryo-EM structure to model the binding of Pn3a to the down state of VSDII of the $hNa_V1.7$/Na_VAb chimera (Figure 6A). Our model is consistent with experimentally obtained data described in previous sections and places both basic residues K22 and K24 in Pn3a in close proximity to D816 and E818, respectively, where they likely form ionic and/or hydrogen bonds with these negatively charged S3−S4 loop residues (Figure 6B). These interactions would likely interfere with S4 gating charge movement by neutralizing necessary acidic side chains or even by repulsing forces of these positive charges, to interfere with channel opening. Consistent with our experimental data showing a slight loss of activity for K22R, this model also suggests that the bulkier and slightly longer arginine may clash with the D816 residue, while an arginine at position 24 would permit closer engagement with E818. Future studies systematically exploring a variety of amino acids, including unnatural amino acids like homo- and nor-arginines, or channel mutagenesis may provide additional experimental evidence supporting this explanation for the observed pharmacological activity of the K22R and K24R analogues.

Furthermore, modeling of Pn3a to the VSDII of $Na_V1.7$ suggests that the side chains of the hydrophobic residues M5, F6, Y27, W30, and F34 in Pn3a are embedded in the membrane, with possible interactions between M5, F6, and W30 in Pn3a and the $Na_V1.7$-specific F813 side chain, supporting the idea that direct channel interactions contribute to the loss of potency we observed *in vitro* in the corresponding $Na_V1.7$ mutant (Figure 6A). Interestingly, ProTx-II shows only slight interaction with F813;[12] however, this residue seems crucial for stabilization of the S3 helix which in turn orients the S3−S4 loop residues to permit close interactions with ProTx-II. In comparison, the glycine residue in $Na_V1.5$ (corresponding to F813 in $hNa_V1.7$) seems to result in a less polar surface in the S3−S4 loop binding region, providing an explanation for ProTx-II having a lower affinity for $Na_V1.5$.[12] W24 in ProTx-II is one of the few residues making intimate contacts with $Na_V1.7$,[12] and the molecular models suggest that Pn3a M25 and Y27 play a similar role, making hydrophobic contacts with the receptor L770 and L812 and the side chain Y27 establishing a hydrogen bond with the backbone carbonyl of L812. Additionally, our model indicates hydrophobic contacts between VSDII L814 and Pn3a W30 and F34 (Figure 6A). The side chain of Pn3a W30 therefore potentially interacts

https://dx.doi.org/10.1021/acsptsci.0c00002
ACS Pharmacol. Transl. Sci. 2020, 3, 535−546

with the first two residues of the S3−S4 segments as well as the membrane, and this central role is supported by the loss of inhibition measured experimentally when W30 is mutated to alanine (Table 1). Future studies on further $Na_V1.7$ mutant channels including D816, E818, L770, L812, and L814 mutants will be necessary to confirm the roles of these residues in Pn3a activity at $Na_V1.7$. Similarly, mutagenesis experiments to introduce $Na_V1.7$-like residues into other $Na_V1.X$ channels could be used to confirm importance of individual channel residues in potency and selectivity of Pn3a.

According to the model, D8 is positioned over the head groups of the lipid membrane, which presumably contains negatively charged moieties.[44,45] Our data suggests that a negative charge at position 8 is poorly tolerated near the lipid head groups, whereas an uncharged polar residue or a basic residue with a long side chain is preferred; indeed, this aligns with our experimental findings that D8N and D8K show improved membrane binding properties and an increased potency at $Na_V1.7$ (Figures 6C and S5). Similarly, the negative aspartic acid at position 1 of the flexible N-terminus may be affected by repulsive long-range electrostatic interactions of negative charges within the membrane, while the N-terminal lysine of D1K would experience attractive long-range electrostatic effects resulting in higher affinity to the channel-membrane complex as confirmed by the improved potency of D1K at $Na_V1.7$.

In summary, our structure−activity-relationship study of the family 2 peptide Pn3a identifies residues necessary for potent and selective inhibition of $Na_V1.7$. Despite limited sequence similarity to ProTx-II, Pn3a binds to an overlapping site on VSDII, with the large interaction surface of the peptide seeming to drive selectivity over other Na_V subtypes. The Pn3a analogue Pn3a[D8N] was more potent *in vitro* and also displayed more potent analgesic activity *in vivo* in a target engagement model as well as a model of postsurgical pain.

3. MATERIALS AND METHODS

3.1. Sequence Alignment of Pn3a. Amino acid sequences of peptides were aligned using clustal omega and the UniProtKB database (http://www.uniprot.org/; entry IDs: Pn3a: P0DM12; SGTx1: P56855; Hm1a: P60992; Hm1b: P0DOC5; ProTx-II: P83476) and manually corrected for cysteine spacing.

3.2. Structural Alignment of Pn3a. The 2D NMR solution structures of Pn3a (PDB 5T4R),[21] Hm1a (PDB 2N6O),[29] or ProTx-II (PDB 2N9T)[31] were superimposed over the disulfide bonds, using the molecular graphics program PyMol.

3.3. Solid-Phase Peptide Synthesis of Pn3a and Pn3a Analogues. Pn3a and analogues were synthesized using solid-phase peptide synthesis as described previously.[22] Briefly, synthesis was performed on a Symphony automated peptide synthesizer (Gyros Protein Technologies, Inc., Tucson, AZ), using Fmoc protocols. Peptides were released from the polystyrene resin and simultaneously deprotected, precipitated with ice-cold diethyl ether and HPLC-purified. The linear peptides were folded in oxidation buffer containing a mix of oxidized and reduced glutathione for 48 h and then HPLC-purified to obtain the final folded peptide products. The peptides were analyzed via electrospray ionization mass spectrometry using an API2000 system (Applied Biosystems, Foster City, CA) to confirm matching calculated and measured masses (Table S3) and via analytical RP-HPLC using a Hypersil GOLD C18 column (2.1 × 100 mm^2, particle size 3 μm; Thermo Fisher Scientific, Waltham, MA) on a Shimadzu LC20AT (Shimadzu Corporation, Kyoto, Japan) to confirm elution of clean, symmetrical peaks (Figure S6). The peptides were further analyzed for proper folding via 1D NMR (Figure S1) and quantified using a Nanodrop spectrophotometer (Thermo Fisher Scientific, Scoresby, Australia).

3.4. NMR Spectroscopy. To ensure that the Pn3a analogues displayed the same overall fold as native Pn3a, we performed 1D ^1H NMR spectroscopy on a Bruker Avance III 700 MHz NMR spectrometer equipped with a cryo-probe.[46] The samples were prepared at a concentration of 50 μM and dissolved in 95% H_2O/5% deuterium oxide (D_2O). To process the spectra, TopSpin 3.5 (Bruker) was used. Agreement of resonance positions in the NH region of Pn3a-analogues compared to that of the native (and biologically active) Pn3a were used to assess folding.

3.5. Generation of [F823G]$Na_V1.7$ Plasmid. The QuikChange II XL kit (Agilent Technologies, Santa Clara, CA) was used for site-directed mutagenesis on murine *Scn9a* (encoding $mNa_V1.7$) containing plasmids (GenScript, Piscataway, NJ; Accession number NM_001290674, transcript variant 1) according to the manufacturer's instructions to introduce a F823G mutation, equivalent to F813 in $hNa_V1.7$. The vector used was pcDNA3.1-Hygro(+) including CMV and SV40 promoters for mammalian expression and a Hygromycin B resistance gene. PCR and Sanger sequencing of the whole open-reading frame was performed to confirm presence of desired and absence of unwanted mutations.

3.6. Cell Culture. Human embryonic kidney 293 (HEK293) cell lines stably expressing human $Na_V1.1$-$Na_V1.8$ channels (SB Drug Discovery, Glasgow, UK) were cultured in minimal essential medium eagle (MEM; Sigma-Aldrich; Castle Hill, NSW) containing 10% (v/v) fetal bovine serum (FBS; Assay Matrix Pty Ltd.), 2 mM L-glutamine, and selection antibiotics as recommended by the manufacturer. Chinese hamster ovary (CHO) cells stably expressing human $Na_V1.8$ in a tetracycline-inducible system (ChanTest, Cleveland, OH) were cultured in Ham's F-12 containing 10% (v/v) FBS and selection antibiotics as recommended by the manufacturer and $hNa_V1.8$ expression was induced by the addition of tetracycline (1 μg/mL) for 24 h at 27 °C. HEK293 cells stably expressing $mNa_V1.7$ or [F823G]$mNa_V1.7$ were generated by transfection with Lipofectamine 3000 (Thermo Fisher Scientific, Waltham, MA) using 20 μg of plasmid DNA and 30 μL of Lipofectamine 3000, followed by selection of stable clonal cell lines with robust Na_V currents using hygromycin B (100 μg/mL). Cells were grown in an incubator at 37 °C with 5% CO_2 and passaged every 3−4 days (at 70−80% confluency) using TrypLE Express (Thermo Fisher Scientific).

3.7. Whole-Cell Patch−Clamp Electrophysiology. To pharmacologically characterize Pn3a analogues, whole-cell voltage−clamp electrophysiology assays were performed on $Na_V1.1$−$Na_V1.7$ expressing HEK293 cells and $Na_V1.8$ expressing CHO cells using the automated electrophysiology platform QPatch-16X (Sophion Bioscience, Ballerup, Denmark) as previously described.[47]

The extracellular solution (pH 7.4; osmolarity 305 mOsm) contained the following: NaCl 70 mM (140 mM for $Na_V1.1$−1.3, $Na_V1.6$, and $mNa_V1.7$/F823G), choline chloride 70 mM (0 mM for $Na_V1.1$−1.3, $Na_V1.6$, and $mNa_V1.7$/F823G), KCl 4 mM, $CaCl_2$ 2 mM, $MgCl_2$ 1 mM, HEPES 10 mM, and glucose 10 mM. The intracellular solution (pH 7.3 (adjusted with

https://dx.doi.org/10.1021/acsptsci.0c00002
ACS Pharmacol. Transl. Sci. 2020, 3, 535−546

CsOH); osmolarity 320 mOsm) contained the following : CsF 140 mM, EGTA 1 mM, CsOH 5 mM, HEPES 10 mM, and NaCl 10 mM. Pn3a analogues were diluted in extracellular solution containing 0.05% bovine serum albumin (BSA). All compound effects were compared to solvent controls following 5 min of incubation.

Concentration−response curves were obtained by measuring the inhibition of peak current (I/I_{max}) elicited by a 20 ms test pulse of −20 mV from a holding potential of −90 mV (at 0.05 Hz frequency), using increasing peptide concentrations (each incubated for 5 min after addition). To calculate IC_{50} values, a four-parameter Hill equation with variable Hill slope was fitted to the data using GraphPad Prism v7.00 (San Diego, CA). Current−voltage ($I-V$) curves were generated before and after addition of peptide from a holding potential of −90 mV with a step pulse series (500 ms each, 5 mV increments), ranging from −110 to +55 mV. Conductance (G) at each voltage (V) was calculated with the equation $G = I/(V - V_{rev})$, (with V_{rev} = reversal potential) to obtain the conductance−voltage curves which were fitted with a Boltzmann equation with GraphPad Prism v7.00. Data are presented as the mean ± standard error of the mean (SEM).

3.8. Fluorescence Imaging Plate Reader (FLIPR) Membrane Potential Assay. To assess the concentration−response relationship and Na_V-isoform selectivity of Pn3a-analogues on human $Na_V1.1-Na_V1.8$ channel isoforms, fluorescence imaging plate reader (FLIPR) membrane potential assays were performed on a FLIPR^{TETRA} cellular screening system (Molecular Devices, Sunnyvale, CA) as previously described.[47] Freshly dissociated cells were seeded into clear-bottomed black-walled 384-well imaging plates (Corning, NY) at a density of ∼10 000 cells/well. Growth media was removed from the wells after 48 h, and the adherent, confluent cells loaded with 20 μL/well red membrane potential dye (Molecular Devices) diluted in physiological salt solution (PSS) for 30 min at 37 °C and 5% CO_2. PSS (adjusted to pH 7.4) contained the following: NaCl 140 mM, glucose 11.5 mM, KCl 5.9 mM, $MgCl_2$ 1.4 mM, NaH_2PO_4 1.2 mM, $NaHCO_3$ 5 mM, $CaCl_2$ 1.8 mM, and HEPES 10 mM. Pn3a-analogues were diluted in PSS containing 0.1% BSA and added to the Na_V channel expressing HEK293 cells using the FLIPR^{TETRA}. Cells were incubated for 5 min with peptides prior to addition of 20 μM veratridine ($Na_V1.6$), 60 μM veratridine ($Na_V1.1-1.5$ and 1.7), or 150 μM deltamethrin ($Na_V1.8$) for Na_V channel stimulation. Changes in fluorescence intensity (excitation 515−545 nm; emission 565−625 nm), equivalent to changes in membrane potential, were measured with a cooled CCD camera. Reads were taken every 1 s for 10 s before (baseline values), 300 s after peptide addition, and a further 300 s after addition of Na_V channel activators. PSS containing 0.1% BSA was used as a negative control.

Raw fluorescence values were converted to response over baseline values and a negative control correction was performed using the FLIPR^{TETRA} software ScreenWorks 3.2.0.14 (Molecular Devices). The computed area under the curve (AUC) values over 300 s after activator addition were plotted, and the inhibitory peptide effects analyzed using GraphPad Prism v7.00. To calculate IC_{50} values, a four-parameter Hill equation with variable Hill slope was fitted to the data. All experiments were performed in triplicate for each treatment (three wells per condition) and the assay was performed on at least three separate occasions.

3.9. Analgesic Efficacy of Pn3a and Analogues *In Vivo*. All *in vivo* experiments in mice were performed in accordance with the International Association for the Study of Pain "*Guidelines for the Use of Animals in Research*" and the Australian Code for the Care and Use of Animals for Scientific Purposes.[49] Ethical approval for experiments involving animals was obtained from the University of Queensland animal ethics committee. The behavioral experiments were conducted using male C57BL/6J mice (aged 6−9 weeks; sourced from *Animal Resources Centre*, WA, Australia), housed in groups of 3−4 per cage under 12 h light-dark cycles, with access to standard rodent chow and water *ad libitum*. A blinded observer (unaware of the treatment received by each animal) performed all measurements.

To determine *in vivo* target engagement, efficacy was assessed in the mouse model of OD1-induced spontaneous pain as previously described.[39] For local treatments, vehicle (0.1% BSA in saline) or Pn3a-analogues (1 μM) were coadministered with the α-scorpion toxin OD1 (300 nM) via shallow subdermal i.pl. injection (40 μL) into the right hind paw. For systemic treatments, vehicle or peptides were administered via intraperitoneal (i.p.) injection (10 μL/g; 0.3−3 mg/kg) 10 min before injection of OD1 (300 nM; 40 μL i.pl.). After injection of OD1, mice were transferred to transparent enclosures and videotaped for up to 30 min from below. Spontaneous nocifensive behaviors including licking, shaking, lifting, or flinching of the injected paw was counted by a blinded observer from the video recordings. All data are expressed as mean ± SEM. Statistical significance compared to vehicle controls was determined in GraphPad Prism v7.00 using one-way ANOVA with Dunnett's multiple comparison test.

An *in vivo* mouse model of postsurgical pain was used to assess the analgesic activity of Pn3a and Pn3a[D8N] as described previously.[22] Briefly, during anesthesia, an incision was made through the plantar skin, fascia, and underlying *flexor digitorum brevis* muscle of the right hind paw. To simulate tissue retraction, the muscle was carefully elevated, leaving muscle origin and insertion intact. The wound was closed after hemostasis with two simple interrupted sutures and treated with 5% povidone−iodine solution. The mice were allowed to recover in their home cages until behavioral experiments. After 24 h of recovery, mice were systemically treated with vehicle (0.1% BSA in saline) or peptides administered via i.p. injection (10 μL/g; 1−3 mg/kg) 10 min before measurement of mechanical allodynia. Paw withdrawal thresholds to mechanical stimulation were determined 24 h postsurgery using an electronic von Frey apparatus (Mouse-Met Electronic von Frey, Topcat Metrology Ltd., Little Downham, United Kingdom) as previously described.[22]

3.10. *In Vivo* Locomotor Performance Test. Motor impairment 20 min after peptide administration was measured using the Parallel Rod Floor apparatus (Stoelting Co,Wood Dale, IL) and data analyzed using the ANY-Maze software (Stoelting Co) as described previously.[39] The number of foot slips within 1 min was divided by the distance traveled to obtain the ataxia index.

3.11. Molecular Docking of Pn3a at $hNa_V1.7$. A molecular model of the interaction between Pn3a and $Na_V1.7$ VSDII was proposed by comparative modeling computed using Modeler 9v20[48] and using as templates the NMR solution structure of Pn3a (PDB 5T4R[21]), the cryo-EM

https://dx.doi.org/10.1021/acsptsci.0c00002
ACS Pharmacol. Transl. Sci. 2020, 3, 535−546

structure of the hNa$_V$1.7 (in complex with Huwentoxin-IV; PDB 6J8H; resolution 3.2 Å[43]), and the cryo-EM structure of hNa$_V$1.7-VSDII/Na$_V$Ab chimera in complex with ProTx-II (PDB 6N4R[12]). The six Cα of the cysteine residues of experimental structure of Pn3a and ProTx-II align with 0.5 Å root-mean-square deviation, indicating the scaffold of these two peptides are highly similar. Beside the cysteine framework, the conformation of the loops 1 and 3 of Pn3a and ProTx-II are similar and were used as anchor point to dock Pn3a on Na$_V$1.7 VSDII using the homology modeling approach. A hundred models were built using Modeler, and the model displaying the lowest DOPE score[50] was selected and then energy-minimized using Amber 18 and the FF14SB force field.[51] The Molprobity[51] score of the tmodels is 1.36 (98th percentile), suggesting that it has very good quality.

3.12. Statistical Analysis. Data and statistical analysis was performed using GraphPad Prism v7.00 (San Diego, CA). Statistical significance was determined as a p-value <0.05 (with *, $p < 0.05$; **, $p < 0.01$; ***, $p < 0.001$; ****, $p < 0.0001$) and was calculated using unpaired t-tests (two-tailed), one-way analysis of variance (ANOVA) with either Tukey's multiple comparison test or Dunnett's multiple comparison test or two-way ANOVA with Sidak's multiple comparison test as appropriate, unless otherwise stated. Data are presented as the mean ± standard error of the mean (SEM) of at least three individual measurements.

■ ASSOCIATED CONTENT

Supporting Information

The Supporting Information is available free of charge at https://pubs.acs.org/doi/10.1021/acsptsci.0c00002.

Methods (surface plasmon resonance); supplementary results and discussion (membrane binding properties of Pn3a and analogues); Figures S1−S6; Tables S1−S3; additional references (PDF)

Molecular model that was used to generate Figure 6 (PDB)

■ AUTHOR INFORMATION

Corresponding Authors

Jennifer R. Deuis − *Institute for Molecular Bioscience, The University of Queensland, St. Lucia, Queensland 4072, Australia*; Email: j.deuis@uq.edu.au

Irina Vetter − *Institute for Molecular Bioscience and School of Pharmacy, The University of Queensland, St. Lucia, Queensland 4072, Australia*; orcid.org/0000-0002-3594-9588; Email: i.vetter@uq.edu.au

Authors

Alexander Mueller − *Institute for Molecular Bioscience, The University of Queensland, St. Lucia, Queensland 4072, Australia*; orcid.org/0000-0002-7447-1310

Zoltan Dekan − *Institute for Molecular Bioscience, The University of Queensland, St. Lucia, Queensland 4072, Australia*

Quentin Kaas − *Institute for Molecular Bioscience, The University of Queensland, St. Lucia, Queensland 4072, Australia*; orcid.org/0000-0001-9988-6152

Akello J. Agwa − *Institute for Molecular Bioscience, The University of Queensland, St. Lucia, Queensland 4072, Australia*; orcid.org/0000-0001-9295-5071

Hana Starobova − *Institute for Molecular Bioscience, The University of Queensland, St. Lucia, Queensland 4072, Australia*

Paul F. Alewood − *Institute for Molecular Bioscience, The University of Queensland, St. Lucia, Queensland 4072, Australia*; orcid.org/0000-0001-7454-6522

Christina I. Schroeder − *Institute for Molecular Bioscience, The University of Queensland, St. Lucia, Queensland 4072, Australia*; orcid.org/0000-0002-6737-6374

Mehdi Mobli − *Centre for Advanced Imaging, The University of Queensland, St. Lucia, Queensland 4072, Australia*

Complete contact information is available at: https://pubs.acs.org/10.1021/acsptsci.0c00002

Author Contributions

J.R.D. and I.V. are co-corresponding authors. A.M., J.R.D., and I.V. conceived the study and designed experiments. A.M., H.S., A.J.A., and J.R.D. conducted experiments and analyzed data. Q.K. performed molecular docking. C.I.S., Z.D., P.F.A., and M.M. provided reagents. A.M. and I.V. wrote the manuscript with input from all authors.

Notes

The authors declare no competing financial interest.

■ ACKNOWLEDGMENTS

The authors thank the University of Queensland Protein Expression Facility for technical help with site-directed mutagenesis and plasmid sequencing. A.M. is supported by an Australian Government Research Training Program Scholarship. A.J.A. and H.S. were supported by a University of Queensland International Postgraduate Scholarship. This work was funded by the Australian National Health and Medical Research Council (NMHRC) through a NHMRC Research Fellowship (P.F.A), a NHMRC Career Development Fellowship (APP1162503) awarded to I.V., a NHMRC Early Career Fellowship (APP1139961) awarded to J.R.D., Development Grant (APP1137011, I.V.), and Project Grants (APP1125766, I.V.; APP1162597, M.M.; and APP1080405, C.I.S.). C.I.S. is an Australian Research Council (ARC) Future Fellow (FT160100055).

■ REFERENCES

(1) Gan, T. J., Habib, A. S., Miller, T. E., White, W., and Apfelbaum, J. L. (2014) Incidence, patient satisfaction, and perceptions of post-surgical pain: results from a US national survey. *Curr. Med. Res. Opin. 30*, 149−160.

(2) Cox, J. J., Reimann, F., Nicholas, A. K., Thornton, G., Roberts, E., Springell, K., Karbani, G., Jafri, H., Mannan, J., Raashid, Y., Al-Gazali, L., Hamamy, H., Valente, E. M., Gorman, S., Williams, R., McHale, D. P., Wood, J. N., Gribble, F. M., and Woods, C. G. (2006) An SCN9A channelopathy causes congenital inability to experience pain. *Nature 444*, 894−898.

(3) Fertleman, C. R., Baker, M. D., Parker, K. A., Moffatt, S., Elmslie, F. V., Abrahamsen, B., Ostman, J., Klugbauer, N., Wood, J. N., Gardiner, R. M., and Rees, M. (2006) SCN9A mutations in paroxysmal extreme pain disorder: allelic variants underlie distinct channel defects and phenotypes. *Neuron 52*, 767−774.

(4) Yang, Y., Wang, Y., Li, S., Xu, Z., Li, H., Ma, L., Fan, J., Bu, D., Liu, B., Fan, Z., Wu, G., Jin, J., Ding, B., Zhu, X., and Shen, Y. (2004) Mutations in SCN9A, encoding a sodium channel alpha subunit, in patients with primary erythermalgia. *J. Med. Genet 41*, 171−174.

(5) Faber, C. G., Hoeijmakers, J. G., Ahn, H. S., Cheng, X., Han, C., Choi, J. S., Estacion, M., Lauria, G., Vanhoutte, E. K., Gerrits, M. M., Dib-Hajj, S., Drenth, J. P., Waxman, S. G., and Merkies, I. S. (2012)

Gain of function $Na_V1.7$ mutations in idiopathic small fiber neuropathy. *Ann. Neurol. 71*, 26−39.
(6) Vetter, I., Deuis, J. R., Mueller, A., Israel, M. R., Starobova, H., Zhang, A., Rash, L. D., and Mobli, M. (2017) $Na_V1.7$ as a pain target - From gene to pharmacology. *Pharmacol. Ther. 172*, 73−100.
(7) McKerrall, S. J., and Sutherlin, D. P. (2018) $Na_V1.7$ inhibitors for the treatment of chronic pain. *Bioorg. Med. Chem. Lett. 28*, 3141−3149.
(8) Kingwell, K. (2019) $Na_V1.7$ withholds its pain potential. *Nat. Rev. Drug Discovery*, DOI: 10.1038/d41573-019-00065-0.
(9) Mobli, M., Undheim, E. A. B., and Rash, L. D. (2017) Chapter Seven - Modulation of ion channels by cysteine-rich peptides: From sequence to structure. *Adv. Pharmacol. 79*, 199−223.
(10) Gilchrist, J., Olivera, B. M., and Bosmans, F. (2014) Animal toxins influence voltage-gated sodium channel function. *Handb. Exp. Pharmacol. 221*, 203−229.
(11) Deuis, J. R., Mueller, A., Israel, M. R., and Vetter, I. (2017) The pharmacology of voltage-gated sodium channel activators. *Neuropharmacology 127*, 87−108.
(12) Xu, H., Li, T., Rohou, A., Arthur, C. P., Tzakoniati, F., Wong, E., Estevez, A., Kugel, C., Franke, Y., Chen, J., Ciferri, C., Hackos, D. H., Koth, C. M., and Payandeh, J. (2019) Structural basis of $Na_V1.7$ inhibition by a gating-modifier spider toxin. *Cell 176*, 702−715.
(13) Ahern, C. A., Payandeh, J., Bosmans, F., and Chanda, B. (2016) The hitchhiker's guide to the voltage-gated sodium channel galaxy. *J. Gen. Physiol. 147*, 1−24.
(14) Ahuja, S., Mukund, S., Deng, L., Khakh, K., Chang, E., Ho, H., Shriver, S., Young, C., Lin, S., Johnson, J. P., Jr., Wu, P., Li, J., Coons, M., Tam, C., Brillantes, B., Sampang, H., Mortara, K., Bowman, K. K., Clark, K. R., Estevez, A., Xie, Z., Verschoof, H., Grimwood, M., Dehnhardt, C., Andrez, J. C., Focken, T., Sutherlin, D. P., Safina, B. S., Starovasnik, M. A., Ortwine, D. F., Franke, Y., Cohen, C. J., Hackos, D. H., Koth, C. M., and Payandeh, J. (2015) Structural basis of $Na_V1.7$ inhibition by an isoform-selective small-molecule antagonist. *Science 350*, aac5464.
(15) Israel, M. R., Tay, B., Deuis, J. R., and Vetter, I. (2017) Chapter Three - Sodium channels and venom peptide pharmacology. *Adv. Pharmacol. 79*, 67−116.
(16) Dongol, Y., Caldas Cardoso, F., and Lewis, R. J. (2019) Spider knottin pharmacology at voltage-gated sodium channels and their potential to modulate pain pathways. *Toxins 11*, 626.
(17) Cardoso, F. C., and Lewis, R. J. (2019) Structure-function and therapeutic potential of spider venom-derived cysteine knot peptides targeting sodium channels. *Front. Pharmacol. 10*, 366.
(18) Schmalhofer, W. A., Calhoun, J., Burrows, R., Bailey, T., Kohler, M. G., Weinglass, A. B., Kaczorowski, G. J., Garcia, M. L., Koltzenburg, M., and Priest, B. T. (2008) ProTx-II, a selective inhibitor of $Na_V1.7$ sodium channels, blocks action potential propagation in nociceptors. *Mol. Pharmacol. 74*, 1476−1484.
(19) Wu, B., Murray, J. K., Andrews, K. L., Sham, K., Long, J., Aral, J., Ligutti, J., Amagasu, S., Liu, D., Zou, A., Min, X., Wang, Z., Ilch, C. P., Kornecook, T. J., Lin, M. J., Be, X., Miranda, L. P., Moyer, B. D., and Biswas, K. (2018) Discovery of tarantula venom-derived $Na_V1.7$-inhibitory JzTx-V peptide 5-Br-Trp24 analogue AM-6120 with systemic block of histamine-induced pruritis. *J. Med. Chem. 61*, 9500−9512.
(20) Murray, J. K., Ligutti, J., Liu, D., Zou, A., Poppe, L., Li, H., Andrews, K. L., Moyer, B. D., McDonough, S. I., Favreau, P., Stocklin, R., and Miranda, L. P. (2015) Engineering potent and selective analogues of GpTx-1, a tarantula venom peptide antagonist of the $Na_V1.7$ sodium channel. *J. Med. Chem. 58*, 2299−2314.
(21) Deuis, J. R., Dekan, Z., Wingerd, J. S., Smith, J. J., Munasinghe, N. R., Bhola, R. F., Imlach, W. L., Herzig, V., Armstrong, D. A., Rosengren, K. J., Bosmans, F., Waxman, S. G., Dib-Hajj, S. D., Escoubas, P., Minett, M. S., Christie, M. J., King, G. F., Alewood, P. F., Lewis, R. J., Wood, J. N., and Vetter, I. (2017) Pharmacological characterisation of the highly $Na_V1.7$ selective spider venom peptide Pn3a. *Sci. Rep. 7*, 40883.
(22) Mueller, A., Starobova, H., Morgan, M., Dekan, Z., Cheneval, O., Schroeder, C. I., Alewood, P. F., Deuis, J. R., and Vetter, I. (2019) Antiallodynic effects of the selective $Na_V1.7$ inhibitor Pn3a in a mouse model of acute postsurgical pain: evidence for analgesic synergy with opioids and baclofen. *Pain 160*, 1766−1780.
(23) Klint, J. K., Senff, S., Rupasinghe, D. B., Er, S. Y., Herzig, V., Nicholson, G. M., and King, G. F. (2012) Spider-venom peptides that target voltage-gated sodium channels: pharmacological tools and potential therapeutic leads. *Toxicon 60*, 478−491.
(24) Moyer, B. D., Murray, J. K., Ligutti, J., Andrews, K., Favreau, P., Jordan, J. B., Lee, J. H., Liu, D., Long, J., Sham, K., Shi, L., Stocklin, R., Wu, B., Yin, R., Yu, V., Zou, A., Biswas, K., and Miranda, L. P. (2018) Pharmacological characterization of potent and selective $Na_V1.7$ inhibitors engineered from Chilobrachys jingzhao tarantula venom peptide JzTx-V. *PLoS One 13*, No. e0196791.
(25) Flinspach, M., Xu, Q., Piekarz, A. D., Fellows, R., Hagan, R., Gibbs, A., Liu, Y., Neff, R. A., Freedman, J., Eckert, W. A., Zhou, M., Bonesteel, R., Pennington, M. W., Eddinger, K. A., Yaksh, T. L., Hunter, M., Swanson, R. V., and Wickenden, A. D. (2017) Insensitivity to pain induced by a potent selective closed-state $Na_V1.7$ inhibitor. *Sci. Rep. 7*, 39662.
(26) Murray, J. K., Long, J., Zou, A., Ligutti, J., Andrews, K. L., Poppe, L., Biswas, K., Moyer, B. D., McDonough, S. I., and Miranda, L. P. (2016) Single residue substitutions that confer voltage-gated sodium ion channel subtype selectivity in the $Na_V1.7$ inhibitory peptide GpTx-1. *J. Med. Chem. 59*, 2704−2717.
(27) Lee, C. W., Kim, S., Roh, S. H., Endoh, H., Kodera, Y., Maeda, T., Kohno, T., Wang, J. M., Swartz, K. J., and Kim, J. I. (2004) Solution structure and functional characterization of SGTx1, a modifier of $K_V2.1$ channel gating. *Biochemistry 43*, 890−897.
(28) Bosmans, F., Martin-Eauclaire, M. F., and Swartz, K. J. (2008) Deconstructing voltage sensor function and pharmacology in sodium channels. *Nature 456*, 202−208.
(29) Osteen, J. D., Herzig, V., Gilchrist, J., Emrick, J. J., Zhang, C., Wang, X., Castro, J., Garcia-Caraballo, S., Grundy, L., Rychkov, G. Y., Weyer, A. D., Dekan, Z., Undheim, E. A., Alewood, P., Stucky, C. L., Brierley, S. M., Basbaum, A. I., Bosmans, F., King, G. F., and Julius, D. (2016) Selective spider toxins reveal a role for the $Na_V1.1$ channel in mechanical pain. *Nature 534*, 494−499.
(30) Flinspach, M. S. D., and Wickenden, A. (2016) *Protoxin-II Variants and Methods of Use*, Janssen Biotech, Inc., Horsham, PA.
(31) Henriques, S. T., Deplazes, E., Lawrence, N., Cheneval, O., Chaousis, S., Inserra, M., Thongyoo, P., King, G. F., Mark, A. E., Vetter, I., Craik, D. J., and Schroeder, C. I. (2016) Interaction of tarantula venom peptide ProTx-II with lipid membranes is a prerequisite for its inhibition of human voltage-gated sodium channel $Na_V1.7$. *J. Biol. Chem. 291*, 17049−17065.
(32) Xiao, Y., Blumenthal, K., Jackson, J. O., 2nd, Liang, S., and Cummins, T. R. (2010) The tarantula toxins ProTx-II and huwentoxin-IV differentially interact with human $Na_V1.7$ voltage sensors to inhibit channel activation and inactivation. *Mol. Pharmacol. 78*, 1124−1134.
(33) Agwa, A. J., Lawrence, N., Deplazes, E., Cheneval, O., Chen, R. M., Craik, D. J., Schroeder, C. I., and Henriques, S. T. (2017) Spider peptide toxin HwTx-IV engineered to bind to lipid membranes has an increased inhibitory potency at human voltage-gated sodium channel $hNa_V1.7$. *Biochim. Biophys. Acta, Biomembr. 1859*, 835−844.
(34) Agwa, A. J., Peigneur, S., Chow, C. Y., Lawrence, N., Craik, D. J., Tytgat, J., King, G. F., Henriques, S. T., and Schroeder, C. I. (2018) Gating modifier toxins isolated from spider venom: Modulation of voltage-gated sodium channels and the role of lipid membranes. *J. Biol. Chem. 293*, 9041−9052.
(35) Wang, J. M., Roh, S. H., Kim, S., Lee, C. W., Kim, J. I., and Swartz, K. J. (2004) Molecular surface of tarantula toxins interacting with voltage sensors in K_V channels. *J. Gen. Physiol. 123*, 455−467.
(36) Caldwell, J. H., Schaller, K. L., Lasher, R. S., Peles, E., and Levinson, S. R. (2000) Sodium channel $Na_V1.6$ is localized at nodes of ranvier, dendrites, and synapses. *Proc. Natl. Acad. Sci. U. S. A. 97*, 5616−5620.

(37) Duchen, L. W. (1970) Hereditary motor end-plate disease in the mouse: light and electron microscopic studies. *J. Neurol., Neurosurg. Psychiatry 33*, 238−250.
(38) Burgess, D. L., Kohrman, D. C., Galt, J., Plummer, N. W., Jones, J. M., Spear, B., and Meisler, M. H. (1995) Mutation of a new sodium channel gene, Scn8a, in the mouse mutant 'motor endplate disease'. *Nat. Genet. 10*, 461−465.
(39) Deuis, J., Wingerd, J., Winter, Z., Durek, T., Dekan, Z., Sousa, S., Zimmermann, K., Hoffmann, T., Weidner, C., Nassar, M., Alewood, P., Lewis, R., and Vetter, I. (2016) Analgesic effects of GpTx-1, PF-04856264 and CNV1014802 in a mouse model of $Na_V1.7$-mediated pain. *Toxins 8*, 78.
(40) Agwa, A. J., Henriques, S. T., and Schroeder, C. I. (2017) Gating modifier toxin interactions with ion channels and lipid bilayers: Is the trimolecular complex real? *Neuropharmacology 127*, 32−45.
(41) Diao, L., and Meibohm, B. (2013) Pharmacokinetics and pharmacokinetic-pharmacodynamic correlations of yherapeutic peptides. *Clin. Pharmacokinet. 52*, 855−868.
(42) Di, L. (2015) Strategic approaches to optimizing peptide ADME properties. *AAPS J. 17*, 134−143.
(43) Shen, H., Liu, D., Wu, K., Lei, J., and Yan, N. (2019) Structures of human $Na_V1.7$ channel in complex with auxiliary subunits and animal toxins. *Science 363*, 1303−1308.
(44) Gennis, R. B. (2013) *Biomembranes: Molecular Structure and Function*, Springer Science & Business Media.
(45) Van Meer, G., Voelker, D. R., and Feigenson, G. W. (2008) Membrane lipids: where they are and how they behave. *Nat. Rev. Mol. Cell Biol. 9*, 112.
(46) Kwan, A. H., Mobli, M., Gooley, P. R., King, G. F., and Mackay, J. P. (2011) Macromolecular NMR spectroscopy for the non-spectroscopist. *FEBS J. 278*, 687−703.
(47) Deuis, J. R., Dekan, Z., Inserra, M. C., Lee, T. H., Aguilar, M. I., Craik, D. J., Lewis, R. J., Alewood, P. F., Mobli, M., Schroeder, C. I., Henriques, S. T., and Vetter, I. (2016) Development of a muO-Conotoxin analogue with improved lipid membrane interactions and potency for the analgesic sodium channel $Na_V1.8$. *J. Biol. Chem. 291*, 11829−11842.
(48) Sali, A., and Blundell, T. L. (1993) Comparative protein modelling by satisfaction of spatial restraints. *J. Mol. Biol. 234*, 779−815.
(49) (a) International Association for the Study of Pain. *Guidelines for the Use of Animals in Research*, https://www.iasp-pain.org/Education/Content.aspx?ItemNumber=1518. (b) Australian Government. (2013) *Australian Code for the Care and Use of Animals for Scientific Purposes*, 8th ed., National Health and Medical Research Council, Canberra.
(50) Morris, A. L., MacArthur, M. W., Hutchinson, E. G., and Thornton, J. M. (1992) Stereochemical quality of protein structure coordinates. *Proteins: Struct., Funct., Genet. 12*, 345−364.
(51) Maier, J. A., Martinez, C., Kasavajhala, K., Wickstrom, L., Hauser, K. E., and Simmerling, C. (2015) ff14SB: Improving the accuracy of protein side chain and backbone parameters from ff99SB. *J. Chem. Theory Comput. 11*, 3696−3713.

https://dx.doi.org/10.1021/acsptsci.0c00002
ACS Pharmacol. Transl. Sci. 2020, 3, 535−546